Shocking Permanent Magnet Motors for Naval Applications

D Mathai MEng[a], B Mound MEng[a], P Hart MEng[a]

[a]*GE Energy Power Conversion UK Ltd, Thomson Houston Way, Rugby CV21 1BD England*

*Corresponding Author. Email: ben.mound@ge.com

Synopsis

Electric motors form the basis of most modern Naval vessels' and submarine propulsion systems. Naval platforms require cost effective, power dense, highly efficient, resilient, low noise and reliable propulsion solutions. Permanent magnet motors (PMM) offer higher power density, higher efficiency, and lower noise than conventional induction motors. The permanent magnets require special consideration under temperature and shock load conditions and require analysis, design and validation to inform their suitability for the desired application. Permanent magnet motors are not a new technology and have been widely adopted in numerous applications and have a high technology readiness level. This paper looks at the simulation and tests carried out on a PMM to validate the magnets' shock capability to meet typical Naval underwater shock requirements. PMM topologies will be presented, surface and embedded, noting specifically embedded magnets are inserted into the rotor laminations and bonded with epoxy resin to hold them in position. Finite element analysis was carried out on the embedded permanent magnet motor and the motor geometry has been optimised to improve the shock capability of the magnets. Magnets were tested at various shock levels using a vertical drop test machine and their magnetic properties were checked after each test to confirm they can withstand the shock requirements while remaining magnetised. Additionally, a rotor segment was manufactured and tested on a shock table to validate the shock withstand capability of the magnets and the lamination. This paper will summarise the shock design and validation results for the permanent magnet motor investigated.

Keywords: Permanent magnet motor; Naval; Shock

1 Introduction

Internal design work was conducted to explore future naval motor technology which investigated different types of motor topology at three ratings. This included a compact induction motor (CIM) and three permanent magnet motors: one with surface mounted permanent magnets (SPM) one with embedded permanent magnets and one with interior permanent magnets (IPM). A surface mounted permanent magnet motor has magnets attached to the external surface of a solid rotor. Both embedded permanent magnets and interior permanent magnets have magnets embedded within a laminated rotor; embedded permanent magnet motors have magnets embedded at the surface of the rotor and will look visually very similar to a surface mounted permanent magnet motor; interior permanent magnet motors have magnets embedded within the rotor surface ensuring a cylindrical rotor is created.

The study found permanent magnet motors are more power dense, more efficient, and produce lower noise and vibration than conventional induction motors. This paper further investigates permanent magnet motor technology (specifically EPMM and IPMM) regarding temperature and shock load conditions to determine their suitability for naval applications using finite element analysis. Additionally, magnets were tested at various shock levels using a rotor segment manufactured and tested on a shock table to validate the shock withstand capability of the magnets and the lamination. This paper will summarise the shock design and validation results for the permanent magnet motor.

Authors' Biographies

Dennis Mathai MEng Lead Mechanical Engineer for GE Vernova's Power Conversion business, UK. His work includes designing rotating machines for naval applications.

Benjaman Mound MEng Graduated 2020 from the University of Lincoln with an MEng in Mechanical Engineering. Currently, a Mechanical Engineer for GE Vernova's Power Conversion business, UK. His work includes shock analysis, thermal analysis, and shaft line analysis of naval equipment and machinery.

Peter Hart MEng Graduated 2018 from the University of Exeter with an MEng in Mechanical Engineering. Systems Mechanical Engineer for GE Vernova's Power Conversion business, UK. His work includes shock analysis of naval equipment.

 https://doi.org/10.24868/11210

2 Permanent Magnet Drop Test

The primary purpose of the drop test was to investigate permanent magnet acceleration-induced demagnetisation of small N40UH and N45H permanent magnet samples. Review of the literature found that the demagnetising effects of direct impact acceleration on permanent magnets was well understood, however, these effects have not been fully investigated for acceleration only with no direct impact. Nor had it been investigated in combination with high temperature, which on its own was known to cause irreversible demagnetisation in permanent magnets. Therefore, a drop test was conducted at various impact-free accelerations and temperatures with the goal to extrapolate the results and provide benchmark data to enable motor designers to predict demagnetisation for given shock and temperature criteria.

A typical shock input profile in the form of acceleration and velocity for a large motor is shown in Figure 1. The primary goal of the test is to achieve the first acceleration pulse i.e., a_m, and T_1 corresponding to maximum displacement.

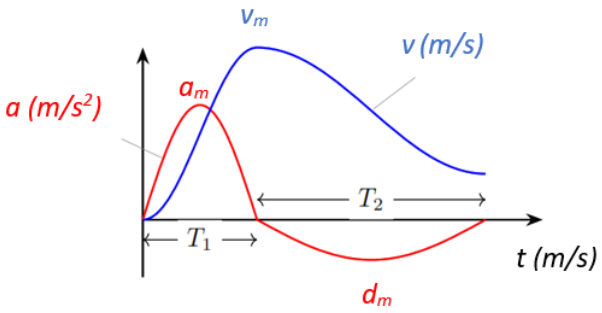

Figure 1: Typical Shock Input Profile for a Motor

Classical or commercial high-strain rate experimental systems, including the Very High Strain-rate testing system and the Split Hopkinson Pressure Bar system were investigated as possible solutions for supplying the required shock input. It was found however, that neither were able to produce the acceleration and/or displacement required and so a drop test was chosen.

Drop tests produce acceleration through direct impact; to produce an impact-free acceleration, a custom rig was created. It consists of a top and bottom plate connected by six outer springs, a "barrel" connected by four upper springs to an upper plate and three bottom springs connected to the base plate as can be seen in Fig. 2. The barrel houses the magnet samples and cartridge heater with additional space to accommodate up to eight copper disks to vary the load and therefore acceleration.

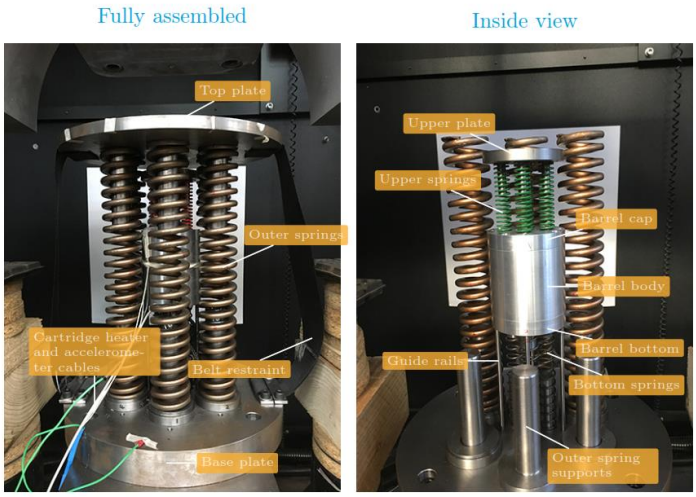

Figure 2: Fully Assembled and Internal View of Drop Test Rig

When released, the striker of the drop tester imparts its potential to the rig's top plate which is connected to the heavy-duty outer springs. These compress and allow the top plate to contact the upper plate, transferring the remaining energy to the upper springs thereby accelerating the barrel.

 https://doi.org/10.24868/11210

The tests were carried out at four different temperatures, ranging from ambient temperature to maximum magnet operating temperature. This was achieved using a small but high–density cartridge heater inserted in the barrel. To vary the output, up to eight weighted copper disks were inserted into the barrel. With this, a good range of acceleration was produced, which includes the target peak acceleration. Figure 3 shows the acceleration profiles produced with varying mass. For Figures 3, 4 and 5, absolute values have not been shown due to security/commercial sensitivity.

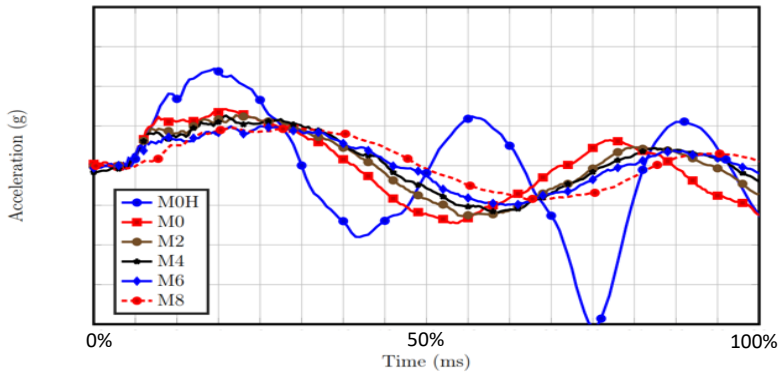

Figure 3: Acceleration Profiles Produced by the Drop Test Rig with Varying Mass

The rig could not achieve the target pulse width of 22 ms, only reaching 50%. However, the peak velocity and displacement are comparable, as shown in Figures 4 & 5, therefore, the acceleration tests largely represent the shock input in terms of acceleration, particularly the first pulse.

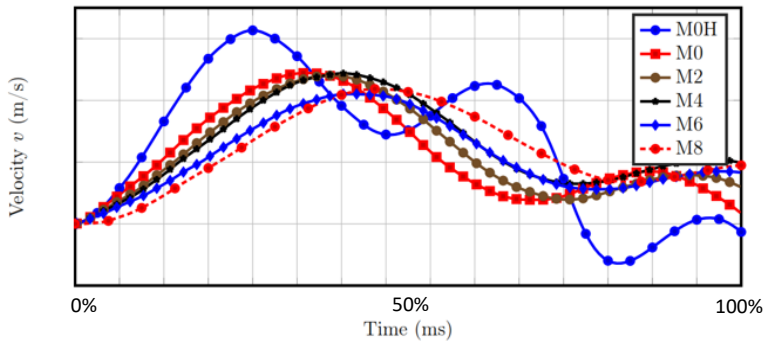

Figure 4: Velocity Profiles Produced by the Drop Test Rig with Varying Mass

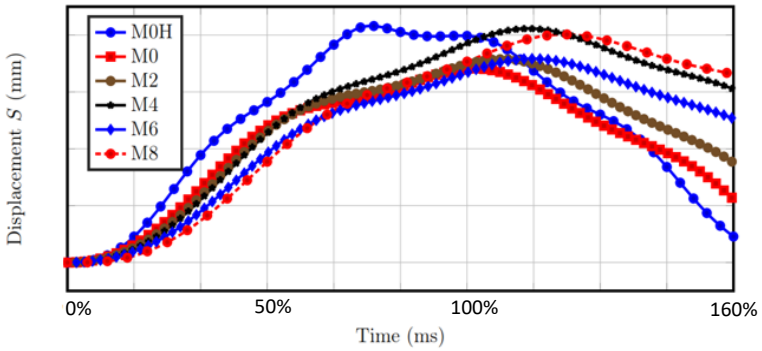

Figure 5: Displacement Profiles Produced by the Drop Test Rig with Varying Mass

Measurements were carried out after the drop tests using an Oxford Vibrating Sample Magnetometer to determine their residual magnetic field strength. It should be noted that only irreversible demagnetisation ct1ould be measured as reversible demagnetisation would require in-situ measurements which were infeasible if not impossible with the current rig design.

The N45H samples were found to exhibit up to 30% demagnetisation at the highest temperature which is three times higher than the maximum operating temperature of the magnet. In contrast with the temperature effect, there is no significant demagnetisation due to acceleration. In comparison, the N40UH samples exhibit only slight (< 5%) demagnetisation, owing to its superior performance at higher temperatures. Again, the demagnetisation

 https://doi.org/10.24868/11210

caused by acceleration is insignificant. Figures 6 and 7 show the magnetic samples' demagnetisation as a function of temperature and acceleration. Once again due to security/commercial sensitivity, absolute values have not been shown for Figures 6 and 7.

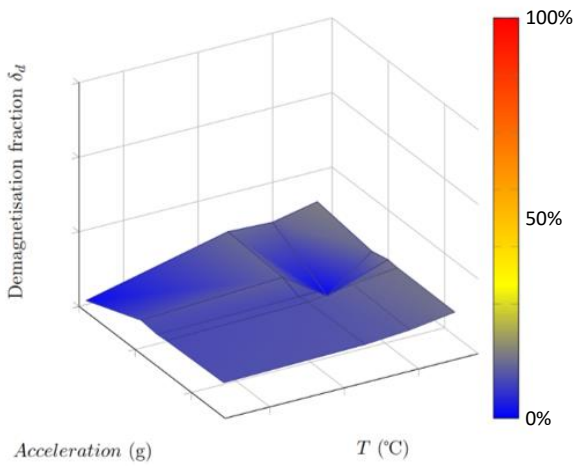

Figure 6: Demagnetisation as a function of temperature and acceleration for N40UH

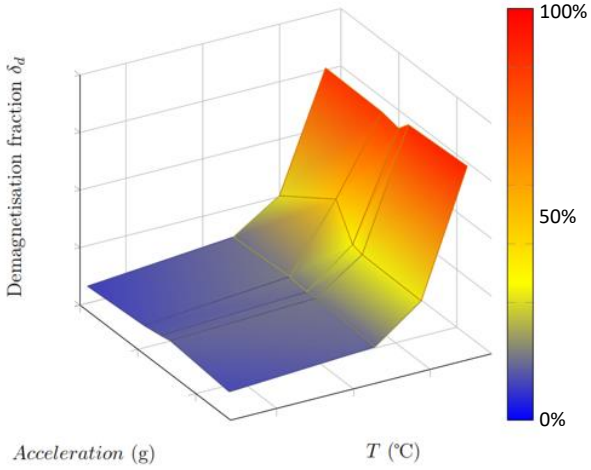

Figure 7: Demagnetisation as a function of temperature and acceleration for N45H

3 Finite Element Analysis of Permanent Magnet Motor

A Finite Element analysis of the permanent magnet motor rotor was completed to determine, via analysis, the ability of the rotor assembly to withstand normal operational and 'rare event' transient loads. The finite element model was used to predict the peak stresses, for both the interior permanent magnet motor and embedded permanent magnet motor rotor designs.

As the assembled rotor core consists of hundreds of thin magnetic steel laminations, compressed via through-bolts, it was modelled in 2D via a Plane Stress analysis. A circumferential span of the rotor, including one pole pair, was modelled; symmetry constraints were applied to the nodes on the circumferentially cut planes. The magnets were bonded, via contact elements, to the top surface of the rotor lamination slot; this is a conservative modelling approach as this ensures the body loads, due to rotational velocity and shock, are transmitted to the thinnest parts of the rotor structure. The laminated rotor is shrunk-fit to discrete arms welded to the shaft; contact elements were used to simulate the shrink-fit. Figure 8 shows the meshed model for the interior permanent magnet motor rotor section.

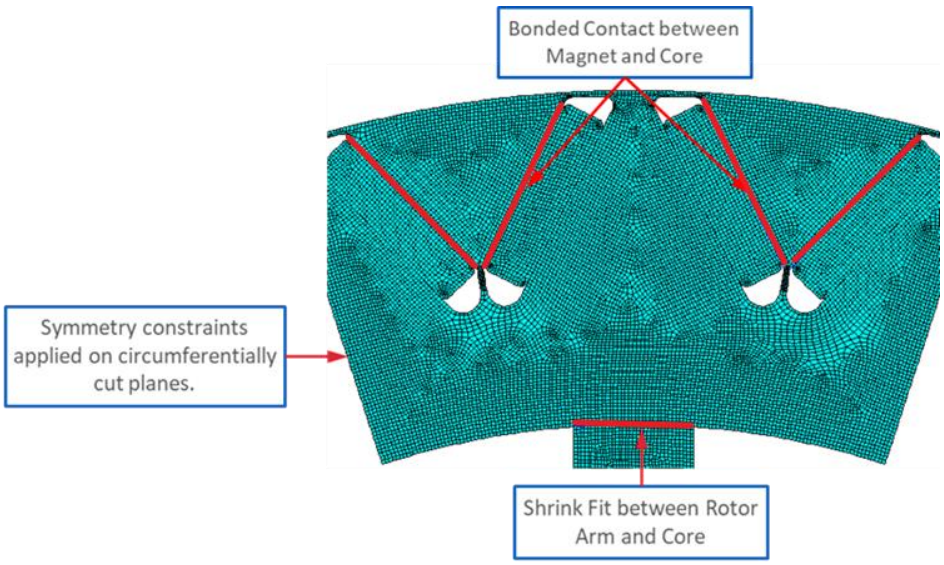

Figure 1: Finite element model of IPMM rotor showing applied boundary conditions.

 https://doi.org/10.24868/11210

The effects of operational and transient loads on the rotor were analysed over four Load Steps:

- Load Step 1: Solve for effects of Shrink Fit. A suitable fit is required to ensure float-off doesn't occur due to inertial loads. The interference fit will generate stresses at the contacting interface, which will distribute radially over the rotor.
- Load Step 2: Solve for effects of Overspeed; this is usually 20% above the maximum operating speed.
- Load Step 3: Maintain Overspeed and solve for Shock Acceleration. Although shock load occurring at overspeed is unlikely, this is a conservative assumption and ensures a suitable shrink fit is chosen that covers all scenarios.
- Load Step 4: Solve for effects of Operational Thermal loads.

The Load Steps were applied in the sequence that would produce the greatest cumulative loading on the rotor. From Figure 9 and 10, the maximum predicted von Mises stress on the interior permanent magnet motor rotor occurred during load step 3 and is localised at the bottom of the slot. This is predominantly due to shrink-fit loads; there is no significant change in predicted stress once the other operational loads are applied. The peak von Mises stress on the magnet, due to shock load, is concentrated at a corner; the predicted stress is within acceptable material limits.

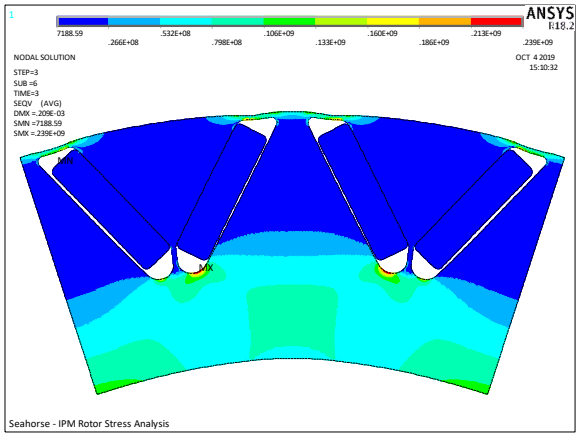

Figure 2: Ansys plot showing predicted von Mises stress at Load Step 3 for the IPMM rotor assembly.

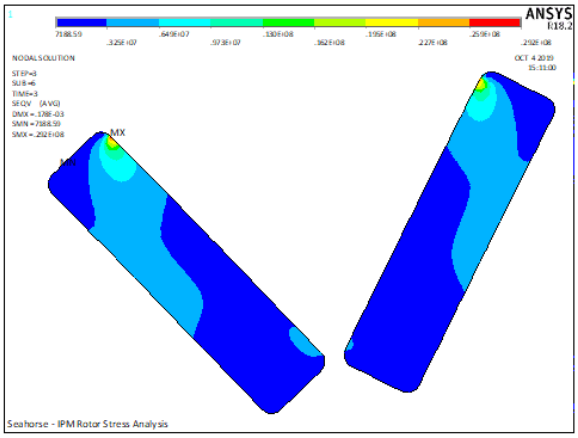

Figure 3: Ansys plot showing predicted von Mises stress at Load Step 3 for the magnet

From Figure 11 and 12 the maximum predicted von Mises stress on the embedded permanent magnet motor rotor occurred during load step 3 and is localised at the bottom rotor and is due to shrink-fit loads; there is marginal change in predicted stress once the other operational loads are applied. The peak von Mises stress on the magnet, due to shock load, is concentrated at a corner; the predicted stress is within acceptable material limits.

 https://doi.org/10.24868/11210

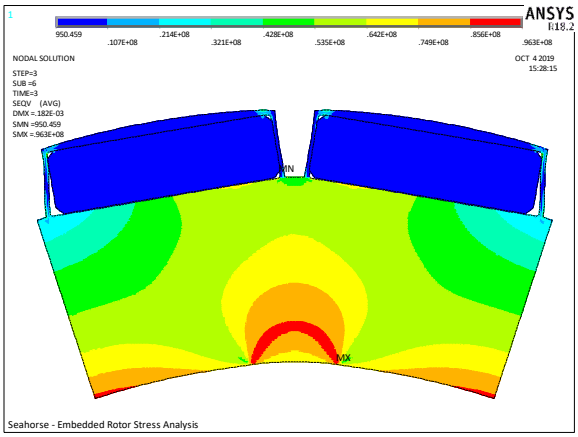

Figure 4: Ansys plots showing predicted von Mises stress at Load Step 3 for the EPMM rotor assembly.

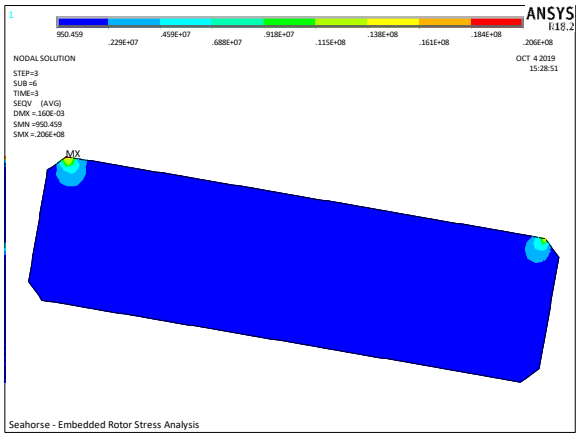

Figure 5: Ansys plot showing predicted von Mises stress at Load Step 3 for the magnet.

4 Shock Test of an Interior Permanent Magnet Rotor

The Power Conversion business designed several interior permanent magnet motors which must withstand a radial shock. As part of the design validation process, a section of the rotor was tested to determine its shock withstand capability. The rotor section consisted of a stack of approximately 1000 laminations, with magnets inserted within discrete slots in the laminated core-pack. The core-pack was compressed between two stainless steel plates; the core compression was maintained via through studs. The test sample consisted of a single pole pair section of the laminated rotor stack, with un-magnetised magnets running the full length of the pole slots; an epoxy resin is used to fill the air gaps between the magnets and the slot. The test was not intended to determine whether shock loads would demagnetise the magnets, therefore only un-magnetised magnet blocks were used for these tests. The assembled rotor section is shown in Figure 13.

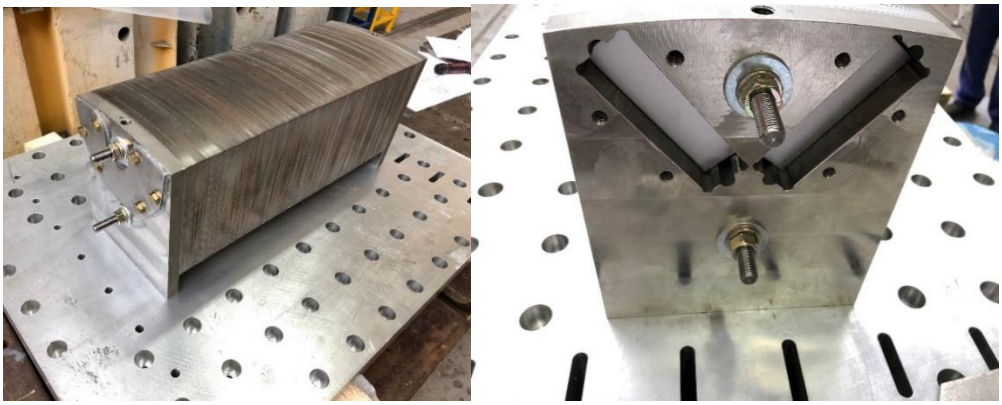

Figure 6: Assembled test sample of the IPMM rotor section

The assembled rotor section was attached to an Electromagnetic Shaker System in its vertical orientation. A control accelerometer was attached as close as practically possible to the specimen's mounting point and a monitor accelerometer was attached on top of the specimen to measure the dynamic response. The test setup is shown in Figure 14.

 https://doi.org/10.24868/11210

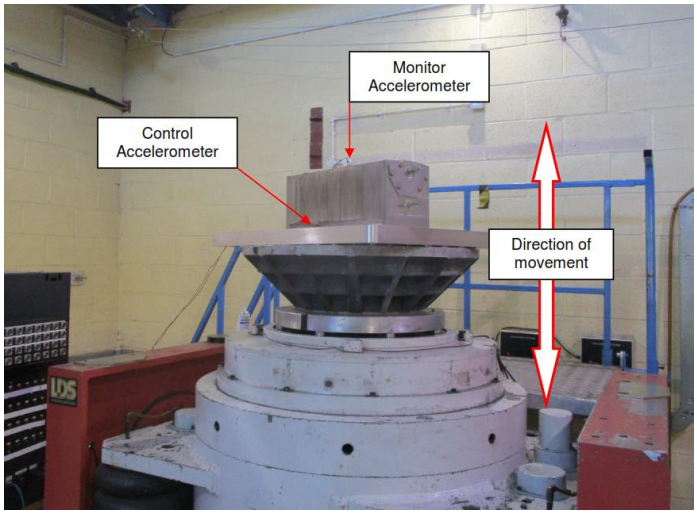

Figure 7: Shock test configuration for test sample.

The test specimen was exposed to a vertical shock acceleration in the positive and negative directions. Figures 15 & 16 show the recorded shock traces, measured on the test specimen. Absolute values are not shown due to security/commercial sensitivity. It must be noted however that both vertical shock accelerations were applied over the same time interval.

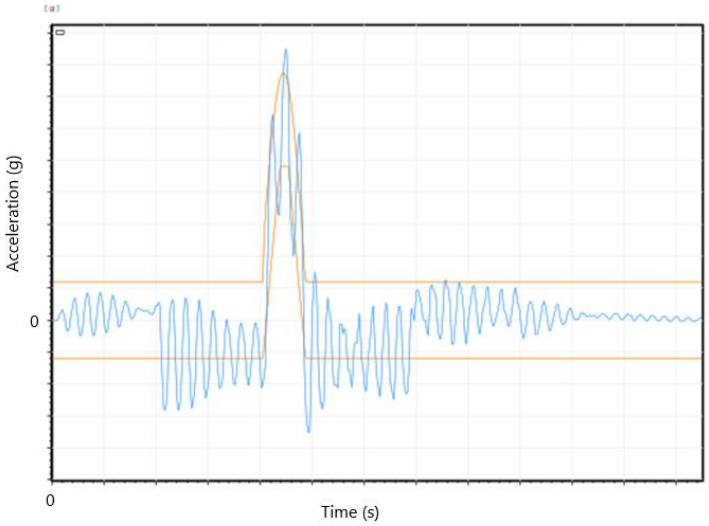

Figure 8: Recorded shock traces showing magnitude and duration of acceleration applied in the vertically positive directions.

 https://doi.org/10.24868/11210

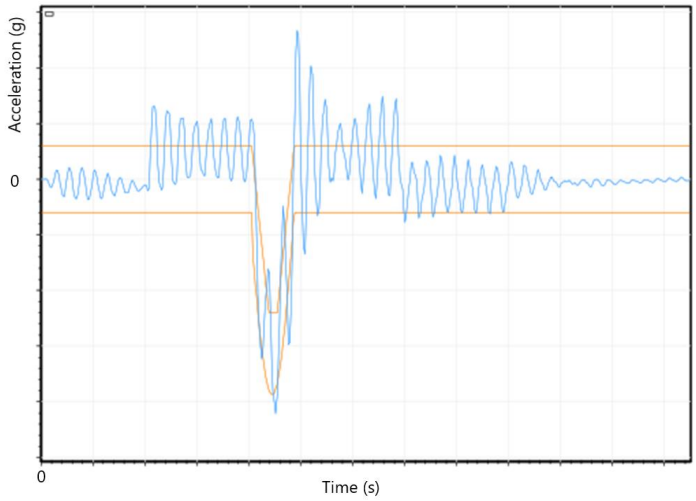

Figure 9: Recorded shock traces showing magnitude and duration of acceleration applied in the vertically negative directions.

Testing was done in accordance with Mil-Std 901D {MIL-S-901D, 1989}; the acceptance criteria was for a Grade A Item. The test acceptance criteria were that:

- The magnets must be intact and must show no signs of damage, such as cracks, which may propagate over time.
- The rotor endplates and core laminations must show no sign of serious damage which will affect its long-term performance.

Inspection of the magnets required a complete strip down of the assembly. Figure 17 shows the stripped-down rotor section: the end plates and compression studs have been removed and laminations have been stripped away exposing the magnets. The magnets, laminations and compression plates showed no signs of damage.

Figure 10: Post test strip-down of test sample: no sign of damage was found on the magnets and rotor components.

5 Conclusion

A drop test rig was designed and built to produce an impact-free acceleration. It was able to accommodate up to eight copper disks to vary the load and thus, acceleration.

The drop tests were performed on two grades of magnets, N45H and N40UH at increasing no-impact accelerations and temperatures to determine their effect on residual magnetisation. It found there is up to 30% and 5% demagnetisation due to exposure to high temperatures in the N45H and N40UH samples respectively whilst the demagnetisation associated with acceleration was insignificant in both sets.

A finite element model was used to predict the peak stresses for an interior permanent magnet motor and embedded permanent magnet motor rotor design. It found lower von Mises stresses occurred in an interior permanent magnet motor and so an IPMM rotor section was created and vertically shock tested in the positive and negative directions. Inspection of the magnets, laminations and compression plates showed no signs of damage, therefore confirming their shock withstand capabilities.

 https://doi.org/10.24868/11210

Acknowledgements

GE Vernova would like to acknowledge The University of Warwick and The University of Nottingham who helped collaborate on the design on the permanent magnet drop test and provided use of their facilities.

References

MIL-S-901D, military specification: shock tests. H.I. (high-impact) shipboard machinery, equipment, and systems, requirements for (17-mar-1989) [s/s by MIL-DTL-901E].

Bibliography

Jun Liu (2017) ‘Optimised Electric System Architecture’ The University of Warwick

 https://doi.org/10.24868/11210